VERSITA

OPTO-ELECTRONICS REVIEW **22**(4), 252–257

DOI: 10.2478/s11772-014-0201-3

Slab waveguide with air core layer and anisotropic left-handed material claddings as a sensor

S.A. TAYA*

Physics Department, Islamic University of Gaza, Gaza, Palestinian Authority

A three-layer slab waveguide with air core layer and anisotropic left-handed material claddings is investigated for sensing applications. Different from the waveguide mode sensors and surface plasmon resonance sensors in which the analyte is placed in the evanescent field region, the proposed sensor contains the sample in the core region that supports the oscillating field. Due to the strong concentration of the electromagnetic field in the analyte medium, the proposed device exhibits unusual sensitivity enhancement. The simulations revealed that the sensitivity improvement of TE_3 mode compared to conventional evanescent wave sensor is approximately a factor of 20.

Keywords: slab waveguides sensors, anisotropic left-handed materials, sensitivity.

1. Introduction

Electric permittivity ε and magnetic permeability μ are the basic physical parameters describing electromagnetic properties of a medium. The propagating behaviour of electromagnetic waves in a medium is determined by its ε and μ which are positive for most natural materials. The phenomenon of negative refraction in media with negative ε and μ was first mentioned in Schuster's book in 1909 [1] and was also introduced by Mandel'shtam in 1940 [2]. The electrodynamics of materials with simultaneously negative values of ε and μ was reported by the Russian physicist Veselago in 1968 [3]. These materials were named left-handed materials (LHMs) because the wave vector **k**, the electric field vector **E**, and the magnetic field vector **H** form a left-handed set in contrast to the conventional materials which were also called right-handed materials (RHMs). The first demonstration of LHMs was achieved by Smith and his co-workers in 2000 [4]. Since then an increasing interest [5–15] on the LHMs properties and possible applications has been exhibited by scientists because of their unconventional electromagnetic properties including reversal of Doppler effect and Cherenkov radiation, negative index of refraction, and unusual nonlinearities.

Slab waveguide sensors have been extensively used in environmental monitoring, medical and pharmaceutical industry, and food technology. Biochemical sensors have been receiving more interest due to their features over other sensors such as high sensitivity, low cost, reduced size, and the possibility of operation in aggressive environments. Tiefenthaler and Lukosz introduced for the first time a planar optical waveguide for gas and humidity sensing by measuring the change in the refractive index of the material contained in the waveguide cover [16]. Since then tremendous advances in slab waveguide sensors have taken place for humidity, gas, chemical, and biochemical sensing [17–34]. Most of these studies have been directed towards enhancing the resolution, miniaturizing the whole system, lowering the cost, and mainly maximizing the sensor sensitivity.

Optical fibre based biosensors have received an increasing interest in the past few years. The most commonly investigated type were enzyme optical fibre based biosensors [21]. Moreover, immunoassay, nucleic acid, and whole cell optical fibre based biosensors have been reported in a considerable number of publications [23]. One of the most commonly proposed sensors was surface plasmon resonance (SPR) sensor and SPR biosensors have become a central tool for characterizing bimolecular interactions [24,25]. Metal-clad waveguide (MCWG) designs were also invested as sensors [26–30]. The structure of a planar MCWG is identical to the normal three-layer slab waveguide consisting of a substrate, a guiding layer, and a cladding with an additional metal layer is introduced between the substrate and the guiding layer. Another significant difference is that MCWGs are usually operated in reflection mode. Fabry-Perot interferometer was also investigated as a sensor [31].

Slab waveguide sensors are known as evanescent wave sensors because the sensing operation is based on the evanescent wave that penetrates the analyte medium from the guiding layer and senses the changes in the refractive index of the analyte. This change in the index of the cladding layer (analyte) is recognized by a change in the effective refractive index of the guided mode. The evanescent field extended from the guiding layer to the surrounding media represents a small fraction of the guided wave and this results in a limited sensitivity of evanescent wave sensors. Such sen-

*e-mail: staya@iugaza.edu.ps

sors can only detect biological substances below 200 nm because the probing depth of the evanescent field has an upper limit of 100–150 nm. Recently the reverse symmetry configuration was proposed to enhance the probing depth [32,33].

Densmore *et al*. [34] have demonstrated that simple thin high contrast index material such as silicon-on-insulation photonic wire waveguide can be used as efficient evanescent sensors.

Despite these efforts much more work has to be done before slab waveguide sensors become commercialized.

A three-layer slab waveguide with air core layer [35–37] and anisotropic lossy dispersive LHM in the claddings is examined as a microwave waveguide sensor in this paper. The air core layer is treated as an analyte and any change in its refractive index is to be detected. The special feature of the proposed slab waveguide sensor is that the analyte to be probed is localized in the core region and is probed by the oscillating field instead of the evanescent field. Therefore, the proposed device avoids the severe drawback of the evanescent field sensors.

2. Dispersion relation and sensitivity

A symmetric three-layer slab waveguide structure including air core layer of the thickness t and the parameters (ε_2, μ_2) is shown in Fig. 1. The surrounding media (cladding and substrate) are assumed to anisotropic, dispersive, and lossy LHM with the permittivity tensor $\ddot{\varepsilon}_1$ and the permeability tensor $\ddot{\mu}_1$. If we consider the optical axis of the claddings to be parallel to the interface (y-z plane), the permittivity and permeability tensors are given by

$$\ddot{\varepsilon}_1 = \begin{bmatrix} \varepsilon_{1x} & 0 & 0 \\ 0 & \varepsilon_{1y} & 0 \\ 0 & 0 & \varepsilon_{1z} \end{bmatrix}, \tag{1}$$

$$\ddot{\mu}_1 = \begin{bmatrix} \mu_{1x} & 0 & 0 \\ 0 & \mu_{1y} & 0 \\ 0 & 0 & \mu_{1z} \end{bmatrix}. \tag{2}$$

The claddings are assumed to have uniaxial anisotropy in which $\varepsilon_{1x} = \varepsilon_{1y}$ and $\mu_{1x} = \mu_{1y}$. Moreover, the LHM claddings are considered to exhibit positive parameters in the transverse directions ($\varepsilon_{1x} = \varepsilon_{1y} > 0$ and $\mu_{1x} = \mu_{1y} > 0$) and negative ones in z-direction ($\varepsilon_{1z} < 0$ and $\mu_{1z} < 0$). In microwave bands, the longitudinal permittivity and permeability are given by

$$\varepsilon_{1z} = \varepsilon(\omega) = 1 - \frac{\omega_p^2}{\omega^2 + i\gamma\omega}, \tag{3}$$

$$\mu_{1z} = \mu(\omega) = 1 - \frac{F\omega^2}{\omega^2 - \omega_o^2 + i\gamma\omega}, \tag{4}$$

where ω_p is the plasma frequency, ω_o is the resonance frequency, γ is the electron scattering rate, and F is the fractional area of the unit cell occupied by the split ring.

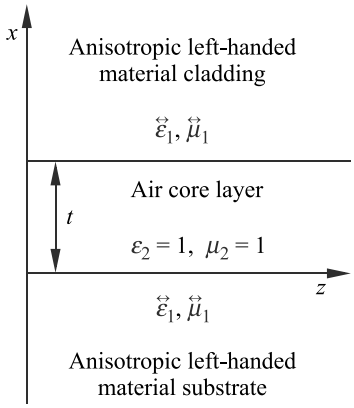

Fig. 1. A three-layer slab waveguide structure including air core layer and anisotropic left-handed material claddings.

For transverse electric (TE) mode the three non-vanishing field components (E_y, H_x, H_z) are related to each other in the anisotropic claddings through the expanded form of Maxwell's equations

$$E_y = -\frac{i}{\omega\varepsilon_{1y}}\left(-i\beta H_x - \frac{\partial H_x}{\partial x}\right), \tag{5}$$

$$H_x = -\frac{\beta}{\omega\mu_{1x}} E_y, \tag{6}$$

$$H_z = \frac{i}{\omega\mu_{1z}} \frac{\partial E_y}{\partial x}, \tag{7}$$

where ω is the angular frequency of the wave and β is the longitudinal propagation constant which is given by $\beta = k_o N$ with k_o is the free space wave number and N is the effective refractive index of the guided mode.

In the air core layer the electric and magnetic field components are related to each other through Eqs. (5)–(7) with ε_2 and μ_2 replacing the tensor elements in these equations. The y-component of the electric field in the slab waveguide is given by

$$E_1 = b_1 e^{-\alpha_1 (x-t)}, \quad x > t, \tag{8}$$

$$E_2 = b_2 \cos(\alpha_2 x - \varphi), \quad 0 < x < t, \tag{9}$$

$$E_3 = b_3 e^{\alpha_1 x}, \quad x < 0, \tag{10}$$

where

$$\alpha_1 = k_o \sqrt{\frac{\mu_{1z}}{\mu_{1x}}(N^2 - \varepsilon_{1y}\mu_{1x})}$$

and $\alpha_2 = k_o\sqrt{n_f^2 - N^2}$ with $n_f = \sqrt{\varepsilon_2\mu_2}$. The coefficients b_1, b_2 and b_3 represent the electric field amplitudes in each layer. φ is a phase constant. When $\mu_{1z}/\mu_{1x} < 0$, the effective refractive index must satisfy $N < \sqrt{\varepsilon_{1y}\mu_{1x}}$ for real α_1. In a similar manner $N < n_f$ for real α_2 and $N > n_f$ for the pure imaginary α_2. Therefore, as $N < \sqrt{\varepsilon_{1y}\mu_{1x}}$ and $N < n_f$ the propagating mode is called TE oscillating guided mode.

On the other hand, as $n_f < N < \sqrt{\varepsilon_{1y}\mu_{1x}}$, the modes are called TE surface modes.

The nonzero tangential component of the magnetic field can be obtained using Eq. (7) in addition to Eqs. (8)–(10),

$$H_1 = \frac{\alpha_1 b_1}{i\omega\mu_{1z}} e^{-\alpha_1 (x-t)}, \quad x > t, \tag{11}$$

$$H_2 = \frac{\alpha_2 b_2}{i\omega\mu_2} \sin(\alpha_2 x - \varphi), \quad 0 < x < t, \tag{12}$$

$$H_3 = \frac{i\alpha_1 b_3}{\omega\mu_{1z}} e^{\alpha_1 x}, \quad x < 0. \tag{13}$$

The field continuity requirement at the interfaces leads to the following dispersion relation

$$\alpha_2 t = 2\tan^{-1}\left(\frac{\mu_2\alpha_1}{\mu_{1z}\alpha_2}\right) + m\pi, \tag{14}$$

where $m = 0, 1, 2, 3, \ldots$ is the mode order.

The effective refractive index of the guided mode depends on a set of waveguide parameters such as refractive indices of the media, thickness of the guiding film, light polarization, and mode order. The structure under consideration is proposed as a microwave waveguide sensor for detecting any changes in the refractive index of the air core layer due to any pollutant. In this case, the effective refractive index changes by ΔN as the index of the air core layer changes by Δn_f. The sensitivity of the proposed sensor is defined as the rate of change of the effective index under an index change of the air film, i.e.,

$$S = \frac{\partial N}{\partial n_f}, \tag{15}$$

where S is the sensitivity.

Differentiating Eq. (14) with respect to N, we get

$$S = \frac{k_o^2\alpha_2\sigma_2 n_f}{tk_o^2 N\sigma_2 + 2\sigma_1\alpha_2}\left[\frac{t}{\alpha_2} + \frac{2\mu_2\alpha_1^2\mu_{1x}\mu_{1z}}{\sigma_2}\right], \tag{16}$$

where

$$\sigma_1 = k_o^2 N\mu_2\mu_{1z}(\mu_{1z}\alpha_2^2 + \mu_{1z}\alpha_1^2), \tag{17}$$

$$\sigma_2 = \mu_{1x}\alpha_1\alpha_2(\mu_{1z}^2\alpha_2^2 + \mu_2^2\alpha_1^2). \tag{18}$$

3. Results and Discussion

Figure 1 shows the proposed microwave slab waveguide sensor in which the analyte is located in the core region. The cladding and substrate are assumed to be identical LHMs. The realization of LHMs is performed by two ways: periodic arrays of metallic wires and split-ring resonators and employing photonic crystals. The claddings are assumed to be fabricated using metallic wires and split-ring resonators. In this case, the fabricated LHM gains many properties from the material inhert properties such as loss, dispersion, and anisotropy. In this work, the LHM claddings are assumed to lossy, dispersive, and anisotropic. Equations (3) and (4) give the experimental model in microwave bands for the permittivity and permeability of the LHM claddings. The experimental values of the coefficients appearing in these equations are $F = 0.56$, $\omega_o = 2\pi\times 4GHz$, $\omega_p = 2\pi\times 10GHz$, and $\gamma = 0.012\omega_p$. Uniaxial anisotropic LHMs are assumed in which $\varepsilon_{1x} = \varepsilon_{1y} = 2.25$ and $\mu_{1x} = \mu_{1y} = 1$. The longitudinal elements of the permittivity and permeability of the LHM claddings are negative and obey the experimental relations given by Eqs. (3) and (4). Both ε_{1z} and μ_{1z} are found to be negative in the frequency band $4GHz < \omega < 6GHz$. The dispersion relation can now be solved numerically for the effective refractive index and the dispersion curves which show the dependence of the effective index on the frequency can be plotted. The numerical solution of the dispersion relation showed the existence of TE_1, TE_2, $TE_{3,\ldots}$ oscillating guided modes. The fundamental guided mode (TE_0) was not found. It was reported in the literature that the guided mode TE_0 cannot be found for any frequency in LHM guiding layer surrounded by linear dielectric media. If one of the surrounding materials has a kerr-type nonlinear refractive index, the fundamental guided mode was found to exist [13]. The dispersion curves of the first oscillating guided mode are plotted in Fig. 2 for different values of the air film thickness. Oscillating guided modes, as well as surface modes were found to exist in the proposed structure because of the anisotropy of the LHM claddings [35]. As can be seen from Fig. 2, the effective index of TE_1 mode is small and ranges between 0 and 1.0. The operating frequency band in which TE_1 mode exists is dependent on the thickness of the guiding layer. The effective index increases as the frequency increases which shows a normal dispersion behaviour and the group velocity ($v_g = d\omega/d\beta$) is positive. Moreover, v_g becomes faster as the frequency increases. For the same value of ω, if the thickness of the air core layer

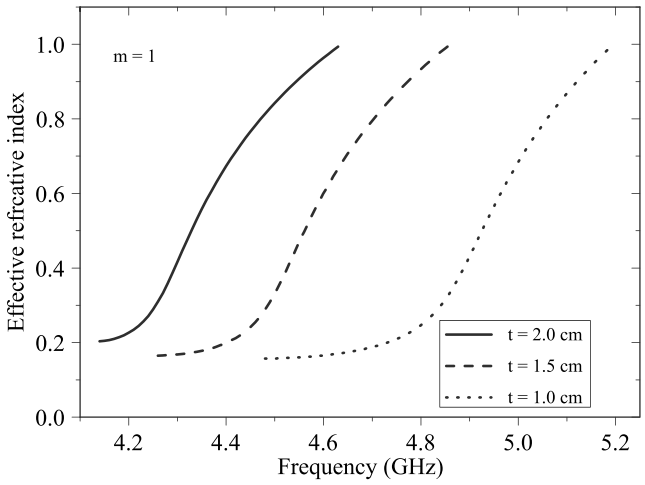

Fig. 2. Dispersion curves of the first guided mode (TE_1) for different air film thicknesses for $\varepsilon_{1x} = \varepsilon_{1y} = 2.25$, and $\mu_{1x} = \mu_{1y} = 1$, $F = 0.56$, $\omega_o = 2\pi\times 4GHz$, $\omega_p = 2\pi\times 10GHz$, $\gamma = 0.012\omega_p$, $\varepsilon_2 = 1$, and $\mu_2 = 1$.

increases, the curves move up indicating an increase in the effective refractive index. However, the operating frequency band becomes wider as the thickness of the air film decreases. This is a significant property in which the core layer thickness can be changed to widen the operating frequency bands and adjust the effective index of the guided mode.

Figure 3 shows the sensitivity of proposed device as a function of the angular frequency for TE_1 mode for the same values of the air film thickness and the same values of the frequency bands illustrated in Fig. 2. Many exciting features can be seen in the figure. The sensitivity increases with ω and peaks at an optimum frequency and then decays as the frequency increases beyond the optimum value. For each guiding film thickness, there is an optimum frequency at which the slab waveguide sensor exhibits its maximum sensing sensitivity. The optimum value of ω is shifted towards higher values as the guiding film thickness decreases. The most important feature can be seen in the maximum value of the sensing sensitivity at the optimum frequency which reaches 1.055 for $t = 2$ cm. Compared to the conventional three-layer slab waveguide in which the analyte is placed in the cladding layer, this value is dramatically high. In the conventional waveguide sensor, the maximum sensitivity can reach up to 0.25 [19,38]. The relatively low sensitivity of the conventional sensors based on the technologies of single and double prism coupling and grating coupling is that a few percent of the mode energy propagates in the cladding medium in which the analyte is placed. On the other hand, the high sensitivity of proposed sensor is attributed to localizing the sample to be probed in the core region in which more than 90% of the guided wave propagates. Therefore, the proposed sensor exhibits dramatically enhanced sensitivity due to the strong concentration of the electromagnetic field in the analyte medium.

In order to study the optimum frequency corresponding to the guiding film thickness, the calculations of the sensitivity were performed for nine different values of t in the range from 0.5 cm to 2.5 cm. The air film thickness *vs*. the corresponding optimum frequency is plotted in Fig. 4 for TE_1 mode. An exponential decay behaviour can be seen from the thickness-optimum frequency curve. This is a normal waveguide behaviour since the thickness of the guiding layer and wavelength of guided wave are usually comparable to each other. Therefore, as the thickness of the guiding film decreases, a shorter-wavelength wave is used for light coupling in.

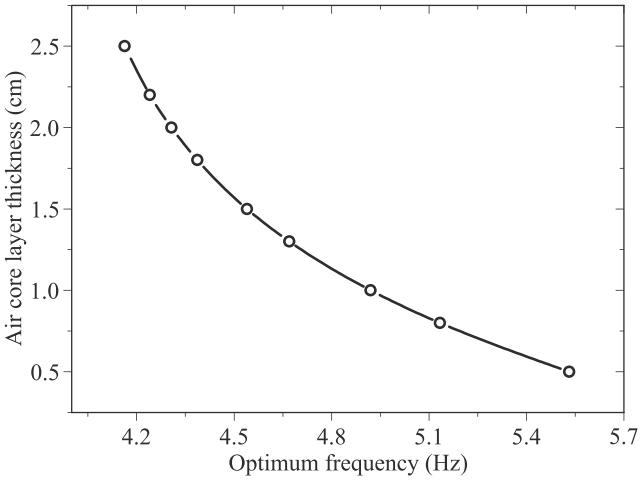

Fig. 4. Thickness of air core layer *vs*. the corresponding optimum frequency for TE_1 mode for $\varepsilon_{1x} = \varepsilon_{1y} = 2.25$, and $\mu_{1x} = \mu_{1y} = 1$, $F = 0.56$, $\omega_o = 2\pi \times 4GHz$, $\omega_p = 2\pi \times 10GHz$, $\gamma = 0.012\omega_p$, $\varepsilon_2 = 1$, and $\mu_2 = 1$.

Figure 5 shows the dispersion curves for the second (TE_2) and third (TE_3) modes for two values of the air core layer thickness. As observed in TE_1 mode, the operating frequency band is crucially dependent on the thickness of the film layer. For $t = 6.5$ cm, the TE_2 mode is found to exist in the frequency band $4GHz < \omega < 6GHz$ whereas for $t = 6$ cm, the band is reduced to $4.11GHz < \omega < 6GHz$. The TE_3 mode

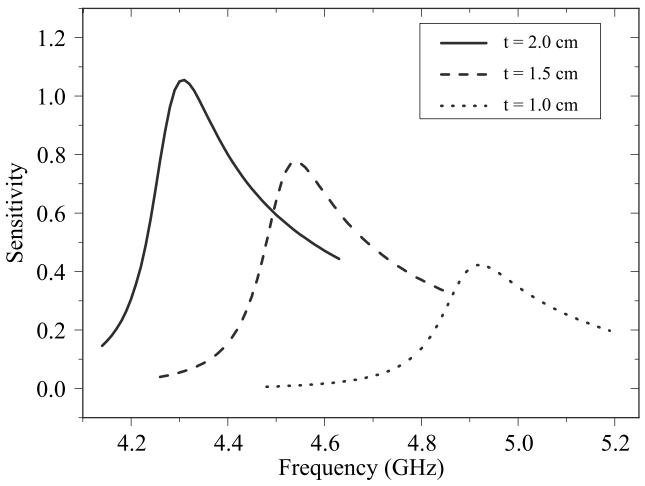

Fig. 3. Sensitivity as a function of the angular frequency for TE_1 mode for different guiding film thicknesses for $\varepsilon_{1x} = \varepsilon_{1y} = 2.25$, and $\mu_{1x} = \mu_{1y} = 1$, $F = 0.56$, $\omega_o = 2\pi \times 4GHz$, $\omega_p = 2\pi \times 10GHz$, $\gamma = 0.012\omega_p$, $\varepsilon_2 = 1$, and $\mu_2 = 1$.

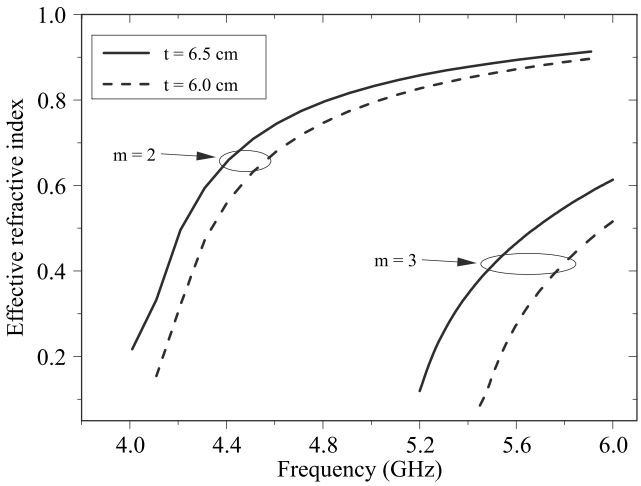

Fig. 5. Dispersion curves of the second and third guided modes (TE_2 and TE_3) for different guiding film thicknesses for $\varepsilon_{1x} = \varepsilon_{1y} = 2.25$, and $\mu_{1x} = \mu_{1y} = 1$, $F = 0.56$, $\omega_o = 2\pi \times 4GHz$, $\omega_p = 2\pi \times 10GHz$, $\gamma = 0.012\omega_p$, $\varepsilon_2 = 1$, and $\mu_2 = 1$.

exists in the operating frequency band $5.2GHz < \omega < 6GHz$ for $t = 6.5$ cm whereas when $t = 6$ cm, the band is reduced to $5.45GHz < \omega < 6GHz$.

The curves in Fig. 5 show the normal dispersion property with positive group velocity. As the frequency increases, their group velocities become faster. As t increases, the curves move up and left.

The sensing sensitivities of the proposed device is plotted for TE_1, TE_2, and TE_3 modes for t = 2 cm, 4 cm, and 6 cm, respectively. The same features observed in Fig. 3 are still available for the sensitivities of higher modes with a strong sensitivity enhancement for higher modes. This behaviour is completely different from that of waveguide mode sensors based on prism and grating coupling in which TE_0 mode corresponds to the highest sensitivity compared to higher modes. This is simply because the evanescent field in the surrounding media is reduced gradually and the wave confinement is enhanced as the mode order increases. Therefore, as the mode order increases, the sensitivity of proposed sensor is dramatically enhanced due to the enhancement of the oscillating field in the core region. As can be seen from the figure, the sensitivities at the optimum frequencies are 1.055, 3.63, and 5.1 for TE_1, TE_2, and TE_3 modes, respectively. The sensitivity improvement of TE_3 mode compared to the conventional evanescent wave sensor is approximately a factor of 20. In order to make a real comparison between two different modes, the sensitivities of TE_2 and TE_3 are plotted in the inset of Fig. 6 for the same value of t. The maximum sensitivities at the optimum frequencies were 2.68 and 5.1 for TE_2 and TE_3 modes, respectively which means that the sensitivity can be almost doubled when moving from a mode to the next one.

Finally, we investigate the behaviour of the sensing sensitivity of the proposed sensor when the anisotropy of the LHM claddings is ignored which is not realistic case. LHMs usually have anisotropy, lossless, and dispersion material feature

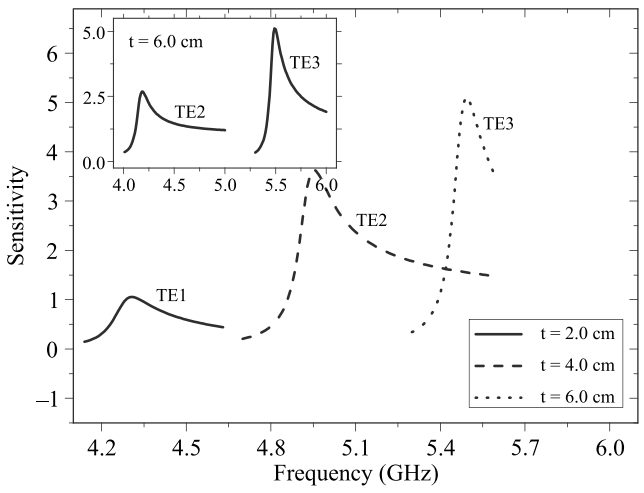

Fig. 6. Sensitivity as a function of the angular frequency for different guided modes for $\varepsilon_{1x} = \varepsilon_{1y} = 2.25$, and $\mu_{1x} = \mu_{1y} = 1$, $F = 0.56$, $\omega_o = 2\pi \times 4GHz$, $\omega_p = 2\pi \times 10GHz$, $\gamma = 0.012\omega_p$, $\varepsilon_2 = 1$, and $\mu_2 = 1$.

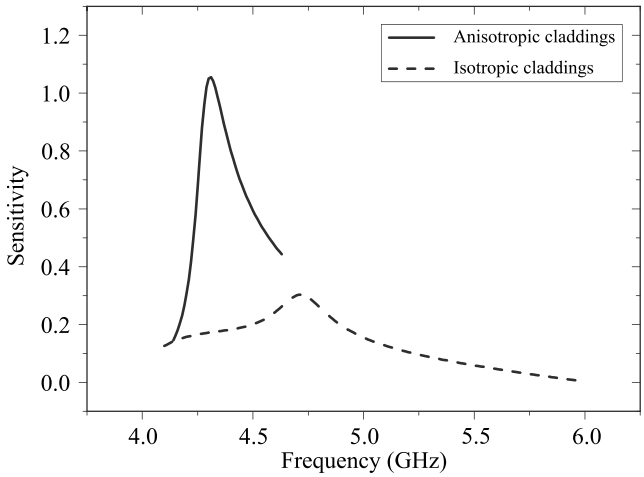

Fig. 7. Sensitivity as a function of the angular frequency for TE_1 mode when the claddings are anisotropic (solid line) and when the LHM anisotropy is neglected (dashed line).

[35]. Figure 7 shows the sensitivity for anisotropic LHM claddings structure and for isotropic LHM claddings structure in which $\varepsilon_{1x} = \varepsilon_{1y} = \varepsilon_{1z} = \varepsilon(\omega) < 0$ and $\mu_{1x} = \mu_{1y} = \mu_{1z} = \mu(w) < 0$. Neglecting the anisotropy of the LHM claddings increases the frequency band in which the TE_1 mode exists and shifts the optimum frequency at which the sensitivity peaks towards a higher value. On the other hand, it leads to a severe reduction in the sensitivity. As can be seen from the figure, the sensitivities at the optimum frequencies are 1.055 and 0.302 for anisotropic and isotropic claddings, respectively. The sensitivity improvement is approximately a factor of 3 when the anisotropy of the LHM is taken into account.

4. Conclusions

A symmetric three-layer slab waveguide was investigated as a sensor for refractometry applications. The structure contains air core layer as an analyte and anisotropic LHM in the claddings. Unusual sensitivity enhancement was observed due to locating the sample in the core region and the anisotropy of the LHM. Many attractive features of the proposed device were detected. For each thickness of the core layer, there is an optimum frequency at which the sensitivity peaks. The optimum frequency is shifted towards higher values as the thickness decreases. The sensitivity is significantly improved by increasing the mode order of the oscillating field in the waveguiding structure. This is in disagreement with the behaviour of the sensitivity of the evanescent mode sensors in which the zero mode corresponds to the highest sensitivity. Considering an ideal LHM of isotropic permittivity and permeability increases the frequency band in which a given oscillating mode exists but leads to a severe reduction in the sensitivity of the proposed device.

The proposed slab waveguide sensor is considered an efficient device for detecting changes in the index of refraction of a sample with considerably high sensitivity which can be enhanced by any factor depending on the mode order of the propagating field.

References

1. A. Schuster, *An Introduction to the Theory of Optics*, E. Arnold, London, 1909.
2. V.M. Agranovich and Yu.N. Gartstein, "Spatial dispersion and negative refraction of light", *Phys-Usp.* **49**, 1029–1044 (2006).
3. V.G. Veselago, "The electrodynamics of substances with simultaneously negative values of Í and µ", *Sov. Phy. Usp.* **10**, 509–514 (1968).
4. D.R. Smith, W.J. Padilla, D.C. Vier, S.C. Nemat-Nasser, and S. Schultz, "Composite medium with simultaneously negative permeability and permittivity", *Phys. Rev. Lett.* **84**, 4184–4187 (2000).
5. S.A. Taya, E.J. El-Farram, and M. M.Abadla, "Symmetric multilayer slab waveguide structure with a negative index material: TM case", *Optik – Int. J. Light Electron Opt.* **123**, 2264–2268 (2012).
6. R. Güther, "Descartes ovaloides for negative refractive indices and their aplanatic cases", *Optik – Int. J. Light Electron Opt.* **119**, 577–583 (2008).
7. S.A. Taya and I.M. Qadoura, "Guided modes in slab waveguides with negative index cladding and substrate", *Optik - Int. J. Light Electron Opt.* **124**, 1431–1436 (2013).
8. M.A. Grado-Caffaro and M. Grado-Caffaro, "Photon mass and negative index of refraction", *Optik – Int. J. Light Electron Opt.* **118**, 353–354 (2007).
9. S.A. Taya and K.Y. Elwasife, "Guided modes in a metal-clad waveguide comprising a left-handed material as a guiding layer", *Int. J. Research and Reviews in Applied Sciences* **13**, 294–305 (2012).
10. I.M. Qadoura, S.A. Taya, and K.Y. El-Wasife, "Scaling rules for a slab waveguide structure comprising nonlinear and negative index materials", *Int. J. Microwave and Optical Technology* **7**, 349–357 (2012).
11. A. Grbic and G.V. Eleftheriades, "Experimental verification of backward-wave radiation from a negative refractive index metamaterial", *J. Appl. Phys.* **92**, 5930–5935 (2002).
12. M.A. Abadla and S.A. Taya, "Characteristics of left-handed multilayer slab waveguide structure", *The Islamic University Journal* (*Series of Natural Studies and Engineering*) **19**, 57–70 (2011).
13. S.A. Taya, H.M. Kullab, and I.M. Qadoura, "Dispersion properties of slab waveguides with double negative material guiding layer and nonlinear substrate", *J. Opt. Soc. Am.* **B30**, 2008–2013 (2013).
14. I.V. Shadrivov, A.A. Sukhorukov, Y.S. Kivshar, A.A. Zharov, A.D. Boardman, and P. Egan, "Nonlinear surface waves in left-handed materials", *Phys. Rev.* **E69**, 016617 (2004).
15. M. Abadla and S.A. Taya, "Excitation of TE surface polaritons in different structures comprising a left-handed material and a metal", *Optik – Int. J. Light Electron Opt.* **125**, 1401–1405 (2014).
16. K. Tiefenthaler and W. Lukosz, "Integrated optical switches and glass sensor", *Opt. Lett.* **10**, 137–139 (1984).
17. R. Horvath, G. Fricsovszky, and E. Pap, "Application of the optical waveguide light mode spectroscopy to monitor lipid bilayer phase transition", *Biosens. Bioelectron.* **18**, 415–428 (2003).
18. S.A. Taya and T.M. El-Agez, "Comparing optical sensing using slab waveguides and total internal reflection ellipsometry", *Turk. J. Phys.* **35**, 31–36 (2011).
19. T.M. El-Agez and S.A. Taya, "Theoretical spectroscopic scan of the sensitivity of asymmetric slab waveguide sensors", *Opt. Appl.* **41**, 89–95 (2011).
20. S.A. Taya, E.J. El-Farram, and T.M. El-Agez, "Goos Hänchen shift as a probe in evanescent slab waveguide sensors", *Int. J. Electron. Commun. (AEU)* **66**, 204–210 (2012).
21. B. Kuswandi, "Simple optical fibre biosensor based on immobilized enzyme for monitoring of trace having metal ions", *Anal. Bioanal. Chem.* **376**, 1104–1110 (2003).
22. S.A. Taya and T.M. El-Agez, "Slab waveguide sensor based on amplified phase change due to multiple total internal reflections", *Turk. J. Phys.* **36**, 67–76 (2012).
23. E. Udd, "An overview of fibre optic sensors", *Rev. Sci. Instrum.* **66**, 4015–4030 (1995).
24. F.C. Chien and S.J. Chen, "A sensitivity comparison of optical biosensors based on four different surface plasmon resonance modes", *Biosens. Bioelectron.* **20**, 633–642 (2004).
25. J. Homola, S.S. Yee, and G. Gauglitz, "Surface plasmon resonance sensors: Review", *Sens. Actuat.* **B54**, 3–15 (1999).
26. H.M. Kullab and S.A. Taya, "Transverse magnetic peak type metal-clad optical waveguide sensor", *Optik – Int. J. Light Electron Opt.* **145**, 97–100 (2014).
27. N. Skivesen, R. Horvath, and H. Pedersen, "Optimization of metal-clad waveguide sensors", *Sens. Actuat.* **B106**, 668–676 (2005).
28. H.M. Kullab, S.A. Taya, and T.M. El-Agez, "Metal-clad waveguide sensor using a left-handed material as a core layer", *J. Opt. Soc. Am.* **B29**, 959–964 (2012).
29. N. Skivesen, R. Horvath, and H. Pedersen, "Peak-type and dip-type metal-clad waveguide Sensing", *Opt. Lett.* **30**, 1659–1661 (2005).
30. H.M. Kullab and S.A. Taya, "Peak type metal-clad waveguide sensor using negative index materials", *Int. J. Electron. Commun.* **67**, 905–992 (2013).
31. S.A. Taya and T.M. El-Agez, "Optical sensors based on Fabry-Perot resonator and fringes of equal thickness structure", *Optik – Int. J. Light Electron Opt.* **123**, 417–421 (2012).
32. N. Skivensen, R. Horvath, S. Thinggaaed, N.B. Larsen, and H. C. Pedersen, "Deep-probe metal-clad waveguide biosensors", *Biosens. Bioelectron.* **22**, 1282–128 (2007).
33. S.A. Taya and T.M. El-Agez, "Reverse symmetry optical waveguide sensor using plasma substrate", *J. Opt.* **13**, 075701 (2011).
34. A. Densmore, D.X. Xu, P. Waldron, S. Janz, P. Cheben, and J. Lapointe, "A silicon-on-insulator photonic wire based evanescent field sensor", *IEEE Photonic Tech. L.* **18**, 2520–2522 (2006).
35. L.F. Shen, J.C. Qiu, and Z.H. Wang, "Guided Modes in a Slab Waveguide with Air Core Layer and Left-handed Materials Claddings", *Proc. Progress in Electromagnetics Research Symposium*, Suzhou, China, 1043–1048 (2011).
36. S.-S. Lo, M.-S. Wang, and C.-C. Chen, "Semiconductor hollow optical waveguides formed by omni-directional reflectors", *Opt. Express* **12**, 6589–6593 (2004).
37. H. Schmidt, Y. Dongliang, J.P. Barber, and A.R. Hawkins, "Hollow-core waveguides and 2-D waveguide arrays for integrated optics of gases and liquids", *IEEE J. Selected Topics in Quantum Electronics* **11**, 519–527 2005.
38. K. Tiefenthaler and W. Lukosz, "Sensitivity of grating couplers as integrated-optical chemical sensors", *J. Opt. Soc. Am.* **B6**, 209–220 (1989).